

STEEL FIBERS FROM WASTE TIRES AS REINFORCEMENTS IN CONCRETE: ANALYSIS OF BOND MECHANISM

Fibras de acero de neumáticos de desecho como refuerzo para concreto: análisis del mecanismo de unión

Yan LI¹, Xiao-Peng WANG¹, Wen-Yang DONG^{2*} and Lan-Qing SHI³

¹ School of Civil Engineering, Jilin Jianzhu University, Changchun, Jilin Province, China.

² Computer Science and Technology Engineering Center, The 964th Hospital, Changchun, Jilin Province, China.

³ School of Civil Engineering, Jilin Jianzhu University, Changchun, Jilin Province, China.

*Author for correspondence: delwine@126.com

(Received: May 2021; accepted: September 2021)

Key words: steel fibers from waste tires, ultimate bond strength, fiber pull-out, drawing failure stage, change of bond stress

ABSTRACT

This paper mainly studies the bond performance between a single recycled steel fiber and concrete, to attain the overall bond strength of recycled steel fibers reinforced concrete. By measuring the load displacement curve of the recycled steel fibers under pullout, we ascertain the maximum bonding stresses of the recycled steel fibers with different depths, angles and shapes while undergoing interfacial pull-out. At the same time, through observations and calculations, the failure phenomena of three stages and the changing trend of bond stresses of recycled steel fibers along the anchorage section are obtained. It is evidenced that the recycled steel fibers reinforced concrete has good interfacial bonding performance. Numerical simulation results of fiber pull-out process via the finite elements provide conditions for the analysis of bond strength of recycled steel fibers reinforced concrete cubes under different circumstances. The above, promotes the recycling of used tires and opens new ways for the green and sustainable use of solid waste.

Palabras clave: fibras de acero de neumáticos de desecho, fuerza de unión final, extracción de fibras, etapa de falla de dibujo, cambio en la tensión de unión

RESUMEN

Este trabajo estudia, principalmente, el desempeño de la unión entre un fibra individual reciclada de acero y el concreto, para obtener la fuerza total de unión entre las fibras recicladas de acero y el concreto. Al medir la curva de la carga de desplazamiento de las fibras de acero bajo extracción, se determina el estrés máximo de los enlaces de las fibras a diferentes profundidades, ángulos y formas, mientras ocurre la extracción interfacial. Al mismo tiempo, por medio de observaciones y cálculos, se obtienen el fenómeno de fractura de tres etapas y la tendencia de los cambios del estrés de unión

de las fibras recicladas de acero en la sección de anclaje. Es evidente que el concreto reforzado con fibras recicladas de acero tiene un buen desempeño de unión interfacial. Los resultados de la simulación numérica del proceso de extracción vía elementos finitos, proveen las condiciones para el análisis de la fuerza de unión de los cubos de concreto reforzado con fibras recicladas de acero bajo diferentes condiciones. Lo anterior promueve el reciclaje de neumáticos usados y abre nuevas posibilidades para el uso verde y sustentable de desechos sólidos.

INTRODUCTION

Waste tires are often termed “black pollution” in the tire industry. The recycling and treatment technology of waste tires has been a worldwide problem, but also a conundrum of environmental protection. Relevant statistics show that there are about 1.5 billion tires discarded every year in the world, and more than 4 million tires are produced every day. Proper use and recycling of the waste tires more effectively and sensibly is the paramount problem faced by the construction industry and environmental protection agencies. In the process of recycling waste tires, composite materials such as steel wires and nylon fibers are typically produced. The steel wire is mainly composed of the bead steel wire, the steel cord fabric and the steel cord. The recovered bead steel wires can be processed into high-strength steel fibers. For convenience, the steel fibers made of recycled bead steel wires are hereinafter referred to as the recycled steel fibers. Adding 0.5% to 2% recycled steel fibers into concrete can form a new class of concrete materials with special performance, which not only protect natural resources and environment, but also provide a new direction for green and sustainable development of buildings. Compared with ordinary steel fibers, the regenerated steel fibers have higher strength and other excellent performances. On the other hand, recycled steel fibers reinforced concrete has been proved to have good compressive strength, shear strength and fatigue resistance by various relevant tests (Aiello et al. 2008, Chen et al. 2018, Jiang et al. 2018, Li et al. 2018). However, the strengthening effect of recycled steel fiber on the bond performance of concrete has not been clearly characterized, which to some extent hinders the engineering application of recycled steel fiber concrete and the process of environmental protection of solid waste recycling.

At present, the research on the strengthening effect of ordinary steel fibers on concrete interfacial bond performance has been basically mature. Deng (Deng 2018) obtained the influence of steel fiber content in the matrix on fibers bonding strength by direct

drawing test. It is confirmed that with the increase of the volume content of steel fibers in the matrix, the peak stress and drawing energy of steel fibers also increase. (Hamoush et al.2010) utilized the single steel fiber pullout test to study the influence of steel fibers with the embedded depth of 6.35-12.7mm on the interfacial bond strength. The experimental results reveal that the peak value of interfacial bond strength between the steel fiber and concrete is inversely proportional to the embedded length of steel fiber, but the peak stress increases with the rise of embedded depth of steel fiber. (Lee et al.2010) studied the influence of the embedded angle of steel fibers upon the interfacial bond strength through several tensile tests of steel fibers. The corresponding results exhibit that when the inclination angles of steel fibers embedded are 30° and 45°, respectively, the maximum drawing peak stress and drawing energy can be achieved. (Zile and Zile 2013). Carried out the pullout tests of single steel fiber, and obtained the bond strength of anisotropic steel fiber embedded in the concrete matrix. It is attested that the bond strength of round straight steel fiber is lower than that of corrugated steel fiber, and the embedded length should not exceed 30mm, so as to prevent bond breakage.

Globally, the research on the bond performance of ordinary steel fibers has been basically established; however, the research on the bond performance of recycled steel fibers is not well developed (Khaloo 1996, Zhou 2000, Song 2004, Aslani 2012, Garcia-Taengua 2016, Hou 2019). The test shows that there is a good bond between the steel fibers and the concrete after the ordinary steel fibers is added into the concrete, so it can effectively bear the force together. There is a lack of definitive research on whether recycled steel fibers can enhance the interfacial bond performance of concrete similar to ordinary steel fibers. In addition, there are some problems in the existing drawing experiments, such as steel fiber fixation is not firm and easy slip seriously affects the accuracy of the test, we have invented a new fixed drawing device with flexible operation and stronger practicability, which can reduce the failure rate of

the test by 60-70 %, save the test time by 20 %, and ensure the accuracy of the test results.

In this study, the recycled steel fiber was mixed into concrete as a new material, and a series of drawing tests were carried out to study the interfacial bond performance between recycled steel fiber and concrete and the key factors affecting the bond performance. And compared with ordinary steel fiber. Furthermore, the load-displacement curves of regenerated steel fibers with different depth, angle and shape, and the ultimate bond strength of regenerated steel fibers under axial were evaluated. Subsequently, the change trend of bond stress along the anchoring section of regenerated steel fiber is calculated, and the interface phenomenon of drawing failure is observed and analyzed. The results of this experiment prove that there are better bond properties between recycled steel fiber and concrete, which provides a theoretical basis for the wide application of recycled steel fiber in engineering practice and is of great significance to further promote the environmental protection process of solid waste recycling.

MATERIALS AND METHODS

Experimental design

In the testing program, nine groups of 100 mm × 100 mm × 100 mm recycled steel fiber reinforced concrete blocks and a group of 100 mm × 100 mm × 100 mm normal steel fiber reinforced concrete blocks were made, each group contains 9 pull-out blocks. The grouping of sample numbers is shown in **Table I**. The diameter of recycled steel fibers utilized in this experimental testing is 1.5 mm, and the tensile strength is more than 1200 MPa; the diameter of normal steel fiber is 1.5 mm, and the tensile strength is

TABLE I. SPECIMEN GROUPING.

Specimen Serial number	Steel fiber type	Buried depth /mm	Embedment angle / °
ZZ20	Round straight	20	0
ZZ30	Round straight	30	0
ZZ40	Round straight	40	0
ZY30	Indentation shape	30	0
ZW30	Hook type	30	0
ZB30	Corrugated shape	30	0
XZ20	Round straight	30	20
XZ30	Round straight	30	30
XZ45	Round straight	30	45
ZC30	Round straight	30	0

800 MPa. Because the recycled steel fibers are taken from the waste tires, the longest steel fiber length can reach 2,000 mm. In this experiment, different lengths (20 mm, 30 mm, 40 mm) of recycled steel fibers are cut out according to different buried depth requirements, and inserted into the cementitious matrix according to the test requirements during pouring. The bonding properties of round straight steel fibers with the cementitious matrix at different embedding depths (20 mm, 30 mm, 40 mm) and different angles (20°, 30°, 45°) were studied, and the bonding properties between special-shaped steel fibers and the matrix were also investigated. According to different characteristics of the outer surface after recycling, the profiled recycled steel fibers can be divided into the corrugated shape, the indentation type and the hook type, respectively.

For the convenience of data recording, we hereby simplify the names of the test blocks. That is, we record ZZ for the round straight recycled steel fiber block with only varying depths, XZ for the round straight recycled steel fibers block with only varying angles, and ZY, ZW and ZB for the indentation shape, the hook type and the corrugated shape recycled steel fibers block. The entire destructive process of the pull-out test of recycled steel fiber reinforced concrete was experimentally observed. In order to reduce the influence of data discretization on data acquisition, the test sample data of each group of test anomalies will be discarded, and the final test results will take the average value of the normal data set. The stains on the surface of industrial recycled steel fibers should be cleaned up during the fabrication of standard positive tension specimens. The manufacturing steps of standard positive tension test specimens are as follows: (1) Place the tempered plate under the mold, leave holes in the middle, fix the recycled steel fiber with glue, and polish off the glue after curing. (2) Remove the dirt on the surface of recycled steel fibers. During the pouring process, the vibration of mortar base and steel fiber should be controlled by a certain range and time duration. (3) The test specimen shall be demolded after being placed in the curing room for 24 hours, and then placed in the water tank for curing for 28 days after demolding.

Experimental materials

The required cementitious material for the testing program is a 42.5 ordinary Portland cement, and the volume stability is qualified. The fine aggregates adopt the ISO standard sands, the fineness modulus is 2.3, the mud content is not more than 1%, and the coarse aggregates are well graded gravels. The test

water was resting three-day water, and naphthalene series water reducer was added to increase its workability. The steel fiber is taken from the steel wire of a waste tire, as revealed in **figure 1**. In order to test the change of bonding properties of recycled steel fiber under different embedding angles, the recycled steel fiber was bent with pliers, as shown in **figure 2**. See **table II** for the concrete mix proportion. The pouring shall be carried out in strict accordance with the GB /T 50080-2002, (test method for performance of ordinary concrete mixture), and maintained in the curing room (with the temperature 20 ± 3 °C, and the relative humidity over 95%) for 28 days, as displayed in **figure 3** below. The cube compressive strength of the test concrete is tested, as shown in **figure 4**, and the average compressive strength is 41 MPa.



Fig. 1. The bead wire.



Fig. 2. Bent recycled steel fiber.

TABLE II. CONCRETE MIX PROPORTION.

Cement quantity/(kg/m ³)	Sand/(kg/m ³)	Water/(kg/m ³)	Gravel/(kg/m ³)	Water reducing agent/(kg/m ³)
513	557	195	1185	5.7



Fig. 3. Recovered steel fibers are embedded in the matrix.

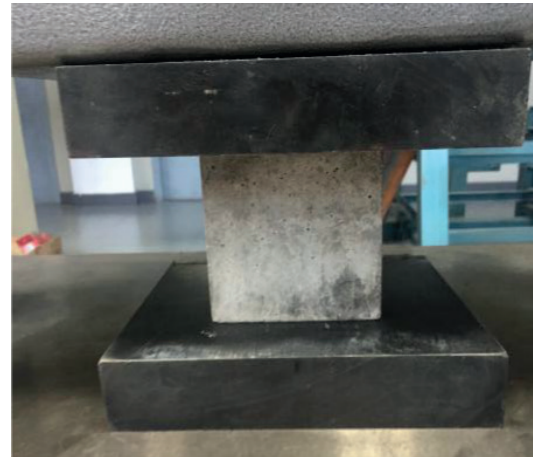


Fig.4. Concrete cube compressive strength test.

Loading scheme

The loading instrument adopts the 50kN electro-hydraulic servo universal testing machine produced by China Changchun Kexin Testing Instrument Co. and carries out relevant tests in the Civil Laboratory of Jilin Jianzhu University. To ensure the accuracy of the testing results, the minimum range is adopted. The recycled steel fiber adopts the cube clamp to fix the cube. The clamp size is slightly larger than the cube specimen. During each test, wedge block shall be inserted in the lower part to prevent the specimen from loosening during the test. The main reason for using this method is that in the process of employing a vise to clamp the lower cube, if the clamping force

is minor, the cube may become loose in the drawing process; if the clamping force is considerable, it may cause the lower cube to be crushed and even affect the test results. In the process of the experiment, the displacement of the recovered steel fiber in the process of drawing is measured by the clip type displacement meter. In the entire process of the experiment, the displacement-controlled loading method is adopted, and the speed is 0.5 mm/min.

The reform and innovation of loading method and experimental equipment

In the case of considering the influence factors of the bond test, after the steel fiber reinforced concrete cubes are completely solidified, the pull-out tests of recycled steel fiber reinforced concrete cubes under different conditions are carried out. In the process of drawing, the clamp displacement meter is employed to measure the displacements. In this test, the displacement-controlled loading is used, the speed is 0.5 mm/min, and the data is collected by a strain collector. The central pull-out test is generally implemented by the pull test machine. The drawbacks of the pull-out device are complex equipment structure, poor sensor accuracy and single operation mode. In order to solve these problems, a new type of fixing and drawing device with flexible operation and strong practicability is proposed in this experiment. See **figure 5** and **figure 6**. The fixture and aluminum sheet are innovatively improved during the test, as exhibited in **figure 7** and **figure 8**, to ensure the accuracy of test data to the highest extent.

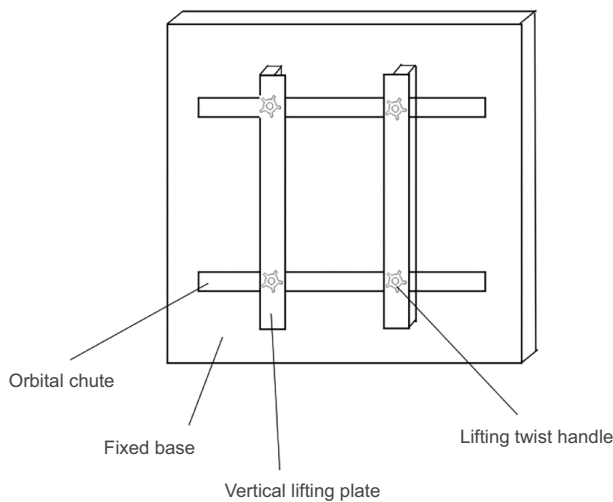


Fig. 5. The face-up diagram of the fixed device of specimen.

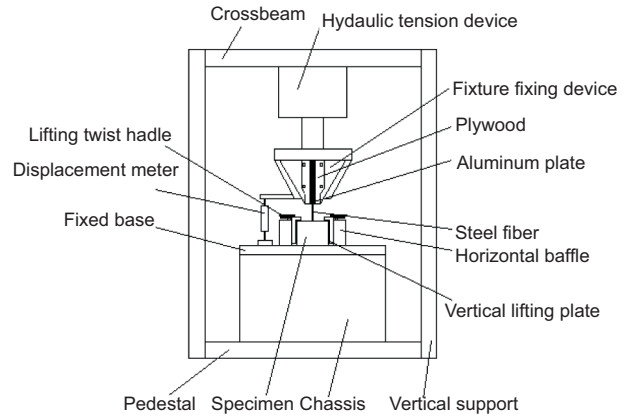


Fig. 6. The structural schematic diagram of a new steel fiber drawing device.

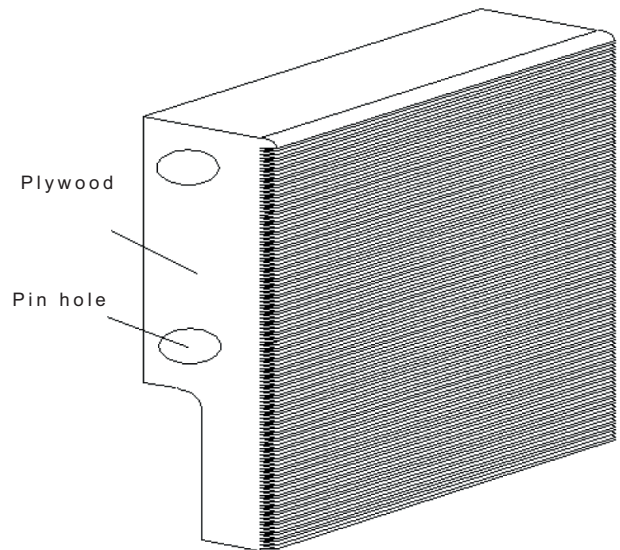


Fig. 7. The schematic diagram of a new type of aluminum plate structure.

In this experimental setting, the new fixing device includes the base, a liftable fixture, and a fixed fixture for immovable specimen. The fixed size can be changed according to the test requirement, and the traditional bench vise can be replaced, which avoids the influence of the traditional bench vise clamping on the test results and the unstable clamping force during the test process. The new drawing device also includes the pedestal, chassis and rack, etc., which features simple equipment, high sensing accuracy and attractive practical value. The new fixture has sharp transverse teeth on the front, upper and lower fixed ports on both sides, which make the

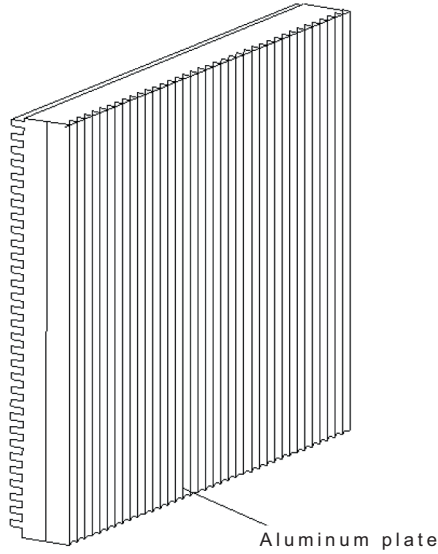


Fig. 8. The schematic diagram of a new splint structure.

fixture firm and reliable, so that the testing success rate is superior. The new type of steel fiber holding aluminum plate used in the experiment adopts the arc tooth structure, which can effectively increase the contact area between steel fibers and aluminum plate, and can effectively increase the friction and biting force. Therefore, the test results are more accurate and the error is significantly reduced compared with the device before our improvement.

The theoretical analysis of steel fiber and concrete drawing model

The interfacial bond strength between the steel fiber and the cementitious matrix is defined as the bond strength of the unit area in between the two phases along the radial direction of the fiber (Mo et al. 2017). The mathematical expression is as follows:

$$f_{fu} = \frac{F_{fu}}{nu_f l_{fe}} \quad (1)$$

where

f_{fu} = the strength of interfacial bond between the steel fiber and the matrix;

F_{fu} = the maximum load when the steel fiber is pulled out (N);

n = the number of embedded steel fibers;

u_f = the girth of the steel fiber cross section;

l_{fe} = the Actual embedding length of steel fiber.

According to the above formula, the tensile strength of a single steel fiber is

$$F_z = f_{fu} u_f l_{fe} \quad (2)$$

where

F_z = the maximum load when a single steel fiber is pulled out (N).

At this point, the maximum tensile stress of the steel fiber takes the form:

$$\sigma_z = \frac{F_z}{A_f} \quad (3)$$

where

A_f = the area of the cross section of the steel fiber (mm^2).

RESULTS AND DISCUSSION

Analysis of interface failure phenomenon

Figure 9 and figure 10 illustrate the fiber-matrix interface failure phenomenon, which can be utilized to analyze the differences of bond properties between the two types of steel fibers and the cementitious matrix. When the matrix interface is damaged, the pulling shape of recycled steel fiber can indirectly reflect the bonding situation.

In the axial drawing process of the round straight steel fiber, there is only a circular void slightly larger than the diameter of the fiber on the surface of the matrix. When the corrugated steel fiber is pulled out, it becomes a small arc-shape and a minor amount of mortar is broken on the interface of the matrix. The diameter of the void is apparently larger than that of the fiber when the corrugated shape and hook-end steel fiber are pulled out. The fiber groove is partly filled with mortar particles, and the interface damage area is considerable. Among them, the hooked

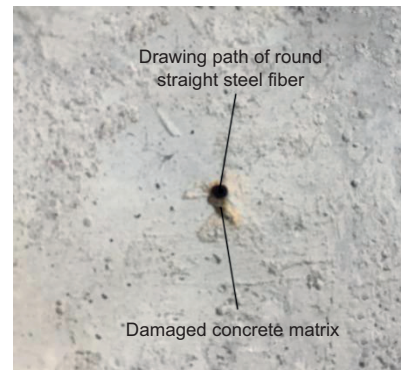


Fig. 9. The axial drawing of round straight steel fiber.

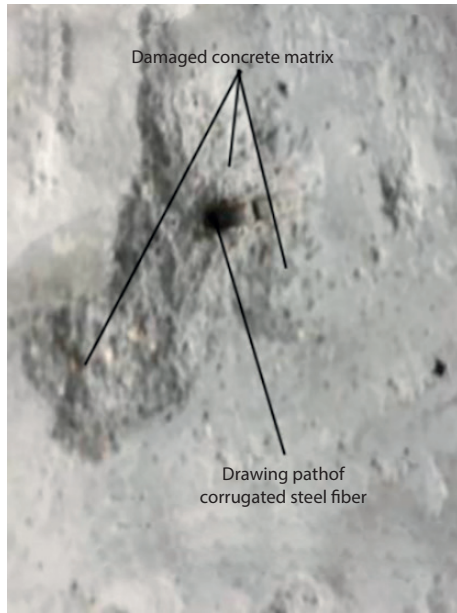


Fig. 10. The axial drawing of the corrugated steel fiber/matrix interface phenomenon.

steel fiber is the most noticeable. The steel fiber in this test is made of steel wire from waste tires, with bronze coating on the surface. The bronze surface gradually wears off due to the friction during the drawing process.

Recycled steel fibers and normal steel fibers

The surface hardness and diameter of recycled steel fiber are close to that of steel fiber. The tensile strength range of bead wire is 1630 ~2150 Mpa compared with the range of steel fiber 380 ~1700 Mpa, it has better material mechanical properties, and has better corrosion resistance than ordinary steel fiber. It can be seen from **figure 11** that the trend of force change between straight normal steel fiber and recycled steel fiber is basically the same when the embedding depth is 30 mm and, as observed in **figure 12**, ZZ30 recovered steel fiber has higher bond strength.

Round straight recycled steel fiber

As observed from **figure 13**, with growing embedded depth, the peak load on each curve increases, and each curve has a rapid rise phase, presenting almost a linear growth. At this phase, the growth rates of ZZ20, ZZ30 and ZZ40 curves are similar. With the increase of displacement, the stress decreases rapidly. The pull-out displacement continues to increase and the curve begins to decline steadily.

When the embedded depth increases by 10 mm and 20 mm, respectively, the peak load increases by

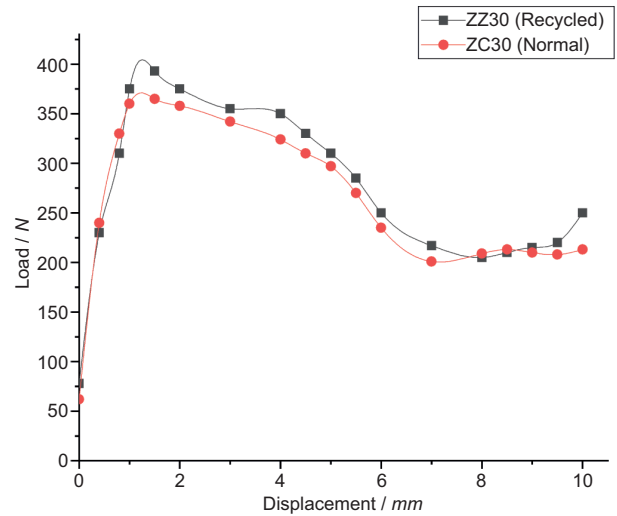


Fig. 11. Comparison of load-displacement curves between recycled steel fiber and normal steel fiber during axial stretching.

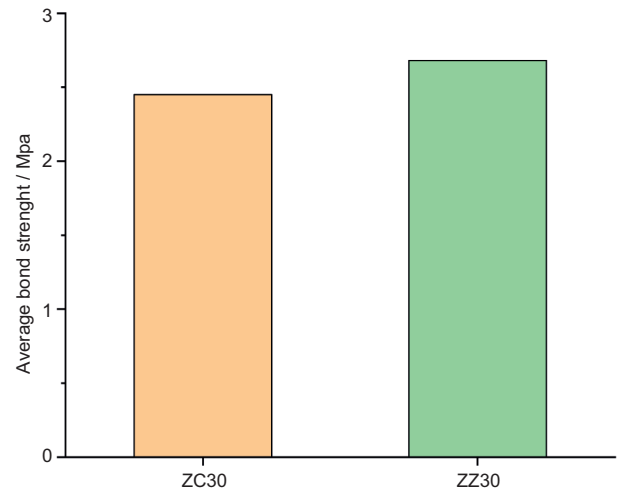


Fig. 12. The ultimate bonding strength of axial drawing of the round straight steel fiber.

37.06% and 84.96%, respectively. The standard deviation of the ultimate bond strength of three groups of specimens is 0.53 MPa. It is witnessed from **figure 14** of the ultimate bonding strength that with the rising embedded depth, the tensile stress between the matrix and the steel fiber increases, and the bond performance improves significantly.

Special-shaped recycle steel fiber

Figure 15 displays the load-displacement curve of a special-shaped steel fiber when the buried depth

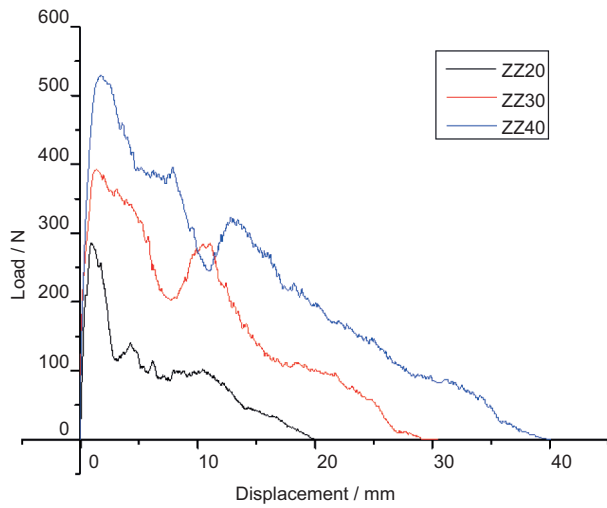


Fig. 13. The load-displacement curve of the round straight steel fibers during axial drawing.

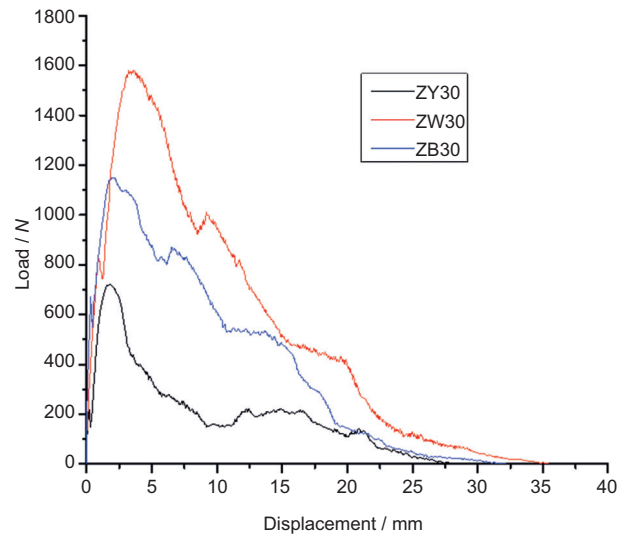


Fig. 15. The load-displacement curve of a special-shaped steel fiber under axial tension.

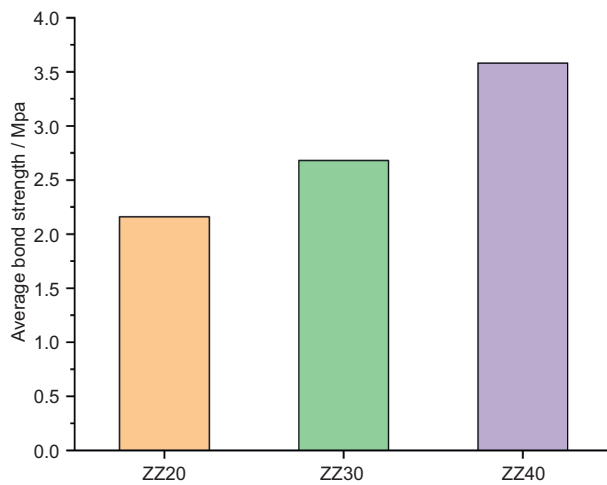


Fig. 14. The ultimate bonding strength of axial drawing of the round straight steel fiber.

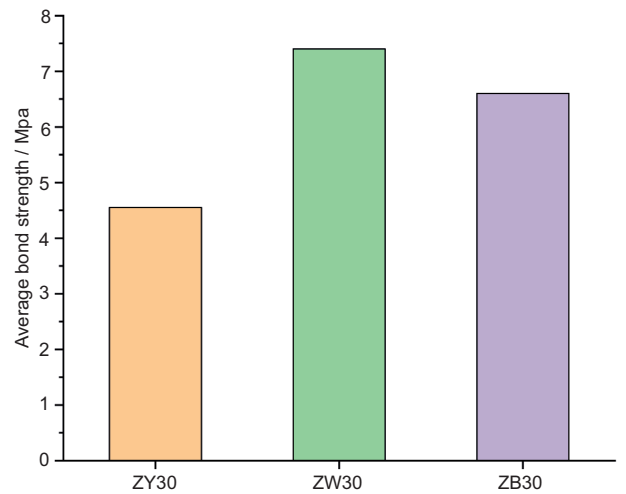


Fig. 16. The ultimate bonding strength of a special-shaped steel fiber under axial tension.

is 30 mm. When the steel fiber is subjected to the drawing force, the curve enters a rapid rise phase; however, when the peak load is reached, the curve drops slightly. When the curve reaches the lowest point of the micro-descending section, due to friction, the curve begins to rise slightly for a second time, and then falls rapidly again until it becomes stable. As observed from **figure 16**, ZW30 has the highest peak load and the best bonding performance. This is because the bent hook recovery steel fiber is pulled out, and the fiber-matrix interface is partially crushed. In addition, due to the presence of the hook, the fiber hook part of the recycled steel fiber will be straightened when it passes through the extraction

channel. As a result, the mechanical biting force greatly increases, and the straightening of the bending hook enhances the pull-out force between the recycled steel fiber and the matrix interface. The standard deviation of the maximum bonding stress of the three groups of specimens is 2.1 MPa, which proves that the shape effect of recycled steel fiber is greater than that of depth and angle.

Stretching in inclined direction

In this study, with the rise of angle, the peak load gradually increases. It is evidenced from **figure 17** that

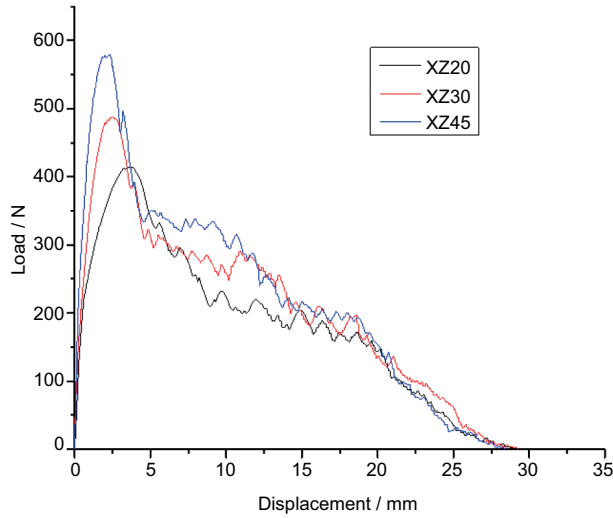


Fig. 17. The load-displacement curve of recycled steel fibers during oblique drawing.

the peak stress of each curve fluctuates within a certain range. With the increase of displacement, each group of curves rises rapidly, of which XZ45 load grows at the fastest speed and XZ20 load rises at the slowest speed. After the displacement reaches 2.5 mm, the variation range of the curve decreases, from steep to gently declining wave shape, and the peak load moves to the right. In the rising stage, the peak load value of XZ45 is 578N; the peak load value of XZ30 is 488N; the peak load value of XZ20 is 414N. The fluctuation and regularity are basically consistent with the variation law of the load-displacement curve versus the burial depth. It is concluded from figure 18

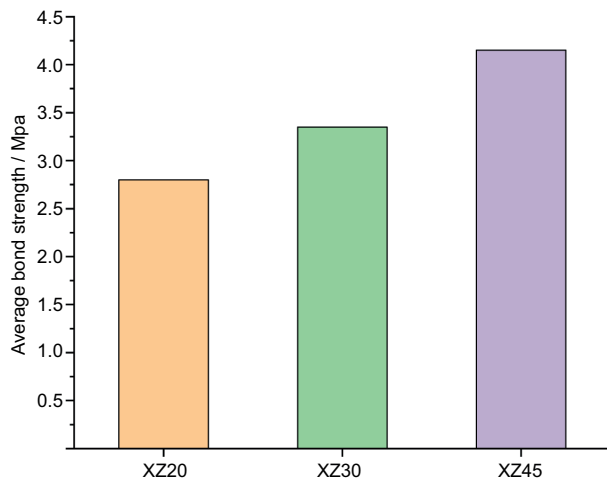


Fig. 18. The ultimate bonding strength of an oblique drawing recovery steel fiber.

that the increases of peak load, adhesive force and angle are positively proportional. The standard deviation of the maximum bonding stress of the three groups of specimens is 0.53 MPa, which proves that the influence of angle on the bond stress is smaller than that of the shape of recycled steel fiber, and the influence of angle and depth on the maximum bonding stress is slightly different.

The main reasons for the direct proportional relationship among the peak load, bond strength and embedded angle are as follows. When the concrete is subjected to external load, cracks will occur in the internal structure, and the steel fiber will bridge the cracks at an angle. (Katz and Li 1995) studied the coupling effect between the axial tension P_{db} and the oblique shear P_b of the round straight steel fiber during oblique drawing, and concluded that:

$$P_f = P_{db} \cdot \cos \theta + P_b \cdot \sin \theta + R\mu \cdot \cos \theta \quad (4)$$

where

P_f = the drawing force of the steel fiber (N);
 P_{db} = the axial drawing load of the steel fiber in oblique drawing(N);
 P_b = the force caused by bending deformation of the steel fiber during oblique drawing (N);
 R = the reaction force of the matrix on the steel fiber due to bending at the pull-out position (N);
 μ = the coefficient of friction.

According to the above formula, P_{db} and P_b will increase with the rise of load after local debonding. When the pull-out force along the fiber direction P_{db} is less than the oblique shear force P_b , the load will continue to rise. The peak load is the largest when the angle is 45°.

Analysis of the change of bond stress with slip in anchorage section

The method of calculation of this article is based upon the mathematical method of Hong and Zhang (2000). It does not calculate the stress between layers, but directly calculates the bond stress of the measuring point. If the strain distribution of the steel fiber in the anchorage zone is sufficiently smooth, there are n units in total, and the length of each section is h , then we write:

$$\varepsilon(x_i + h) = \varepsilon(x_i) + h\varepsilon'(x_i) + \frac{h^2}{2!} \varepsilon''(x_i) + \frac{h^3}{3!} \varepsilon'''(x_i) + o(h^4) \quad (5)$$

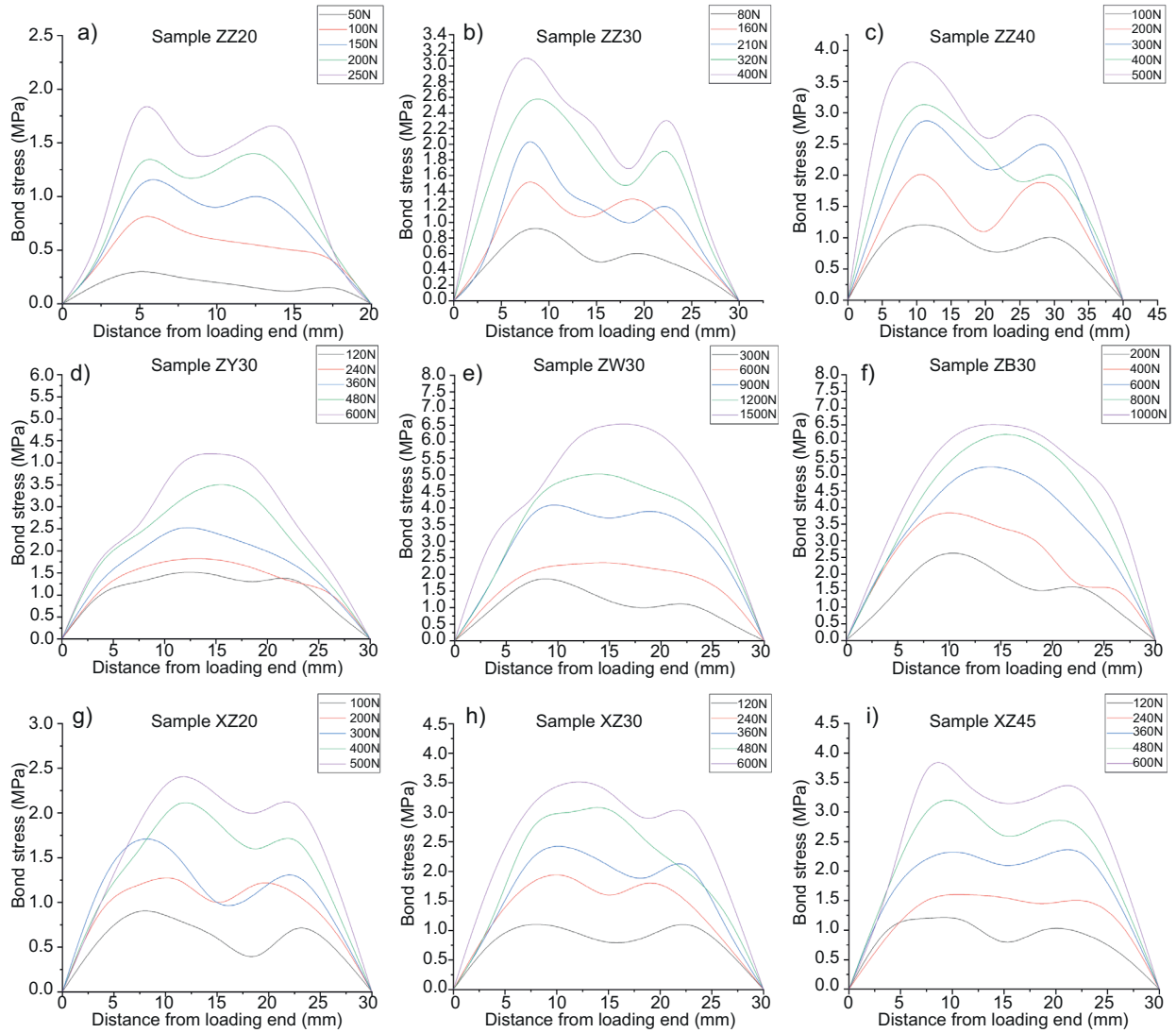


Fig. 19. The distribution curve of bonding stress along the anchorage section.

was utilized to simulate the nonlinear bonding between fibers and the matrix, and a four-node element of COH2D4 shell with bonding layer was established. The damage value was set for material properties, and the energy type was adopted for the damage setting. The energy was calculated from the initial section of the load-displacement curve. In order to consider the fading of the bonding effect after the interface debonding, the bonding unit is automatically deleted after the damage value of the bonding unit is reached. The constraints of the model are applied to the bottom of the matrix model. The matrix elastic modulus $ES = 14000 \text{ N/mm}^2$ and the fiber elastic modulus $ES = 210 \text{ GPa}$. The element modeling is based on (Li and Mobasher 2015), and the

thickness is 0.05 mm . The parameters are based on as exhibited in **table III**.

TABLE III. THE UNIT PARAMETERS.

$(E / K_{nn}) /$ (MPa)	$(G_{ss} / K_{tt}) /$ (MPa)	$(G_2 / K_{tt}) /$ (MPa)	$G_f /$ (N/mm)
52	52	0	0.03

Model analysis and validation

The model dimensions are displayed in **figure 20**. In this model, the embedded depth of the steel fiber is 30 mm , and the displacement load set in the loading

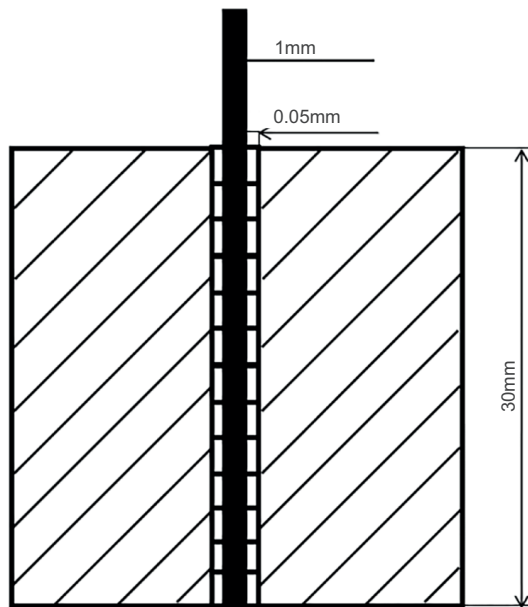


Fig. 20. The drawing model dimension.

step is 5 mm along the axial direction of fiber. The numerical simulation results of the round straight steel fiber are rendered in **figure 21**, **22** and **figure 23**.

The finite element simulation in this section is also an attempt to investigate the bonding mechanism between the fibers and the mortar body as well as the interfacial changes during the pull-out process, so both bonding simulation and experiment are indispensable to study the fiber pull-out. The model is compared with the experimental results to verify the accuracy of the finite element simulation. **Figure 24** shows the comparison between the numerical simulation and the test load-deflection curve. It is witnessed from the figure that when the initial load is minor, the curve of the test block and the curve of the simulation block change linearly; however, the growth rate of the simulated test block is higher than the data obtained by the experimental tests. Currently, both the experimental test block and the simulated test block are in the stage of complete elastic constraint. With the increase of the load, the fluctuation trend of the load decreases rapidly. The simulated test block reveals an inflection point in the load-displacement curve at 385N, and the experimental test block displays an inflection point at 393N; When the displacement is loaded to 8 mm, cement particles or fine sand particles are embedded between steel fiber and matrix due to friction and mechanical extrusion, which increases the mechanical bite force and friction between steel fiber and matrix. There is a lifting section in the late the test

block curve. By analyzing the simulated test blocks, when the bonding interface element is deleted gradually, it indicates that the bonding interface has begun to debond. When the bonding element is about to fade completely, the load begins to decrease. Finally, when the displacement is loaded to 5 mm, the load decreases clearly. In the numerical simulation, the stress of the fibers embedded in the matrix decreases gradually from the top to the bottom. With the increase of the displacement load, the fibers are pulled out continuously and the stress of the fibers gradually reduces.

On this basis, by implementing contrast simulation specimens with the buried depth of 20 mm and 40 mm, respectively, the final numerical simulation results are rendered in **figure 25** and **figure 26**. The comparison between the numerical simulation and the experimental load-deflection curves is revealed in **figure 27** and **figure 28**. The accuracy of the finite element simulation is verified accordingly.

Analysis of interface failure mechanism

Through the analysis of the curves obtained from experiments and finite element simulations, it can be concluded that the failure process of bonding of green fibers can be divided into the following three stages (Krenchel and Shah 1985, Thomas and Ramaswamy 2007, Xu et al.2011, Xu et al. 2012, Zhang et al.2013, Yue et al. 2017, Zhang et al.2019 Zhang et al.2020).

(1) Complete elastic constraint stage. Currently, the interface between the steel fiber and the matrix is in a state of complete bonding. The pull-out resistance at this stage is provided by the interfacial adhesion force. The energy consumption is mainly due to the elastic deformation of steel fibers and bonding interface.

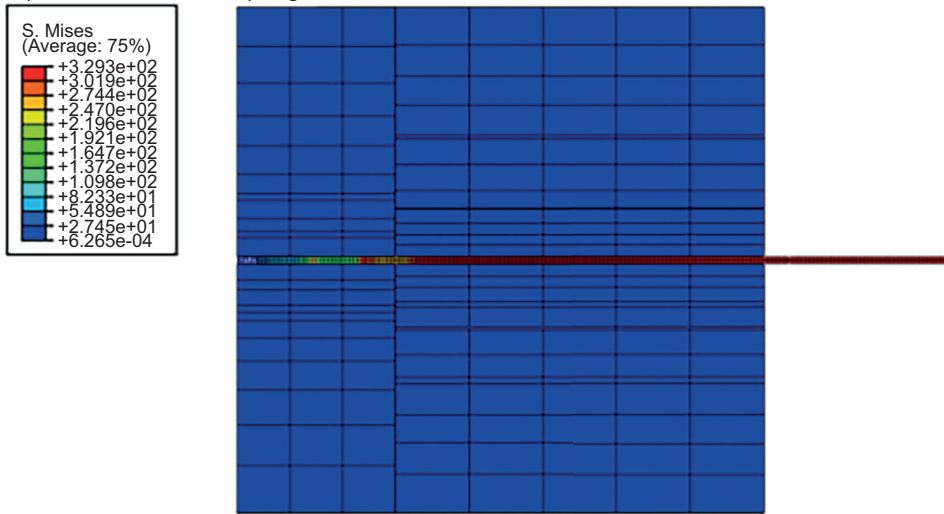
(2) Local debonding stage. In this stage, the failure occurs gradually from the drawing end to the embedding end, and the displacement increases gradually. The pulling resistance at this stage is provided by the interfacial adhesion force and friction force.

(3) Complete debonding stage. Fully unbounded and in the dynamic pull-out stage, the pull-out load decreases with the increase of displacement. The pull-out resistance at this stage is provided by the interfacial friction and fiber deformation.

The deviation analysis

In consideration of the bond performance between the recycled steel fiber and the matrix, a numerical model of the axial tension drawing of the circular steel fiber reinforced concrete cube is established by using the finite element method. By establishing a drawing model to simulate the steel fiber pull-out

a) The initial stress nephogram



b) The intermediate stress nephogram

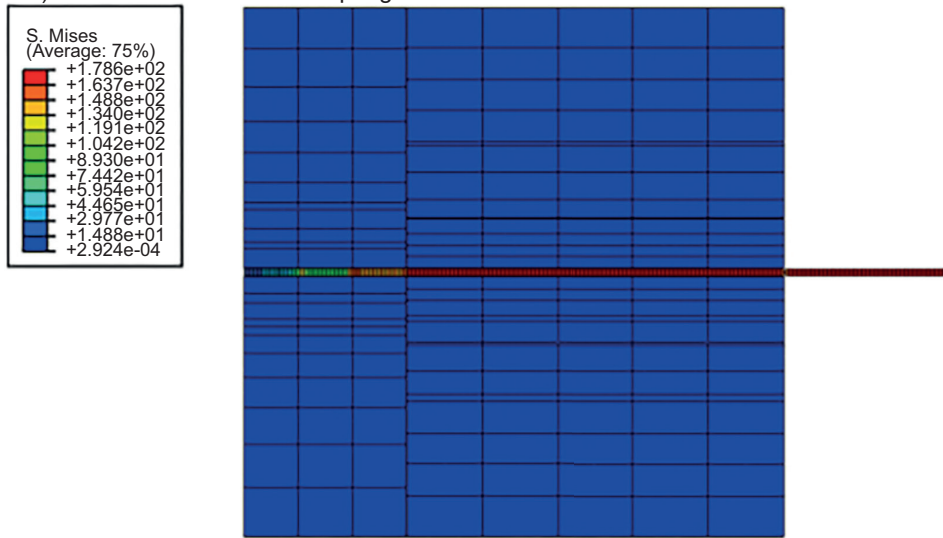


Fig. 21. The stress nephogram of numerical simulation of the steel fiber drawing.



Fig. 22. The fiber drawing stress nephogram.

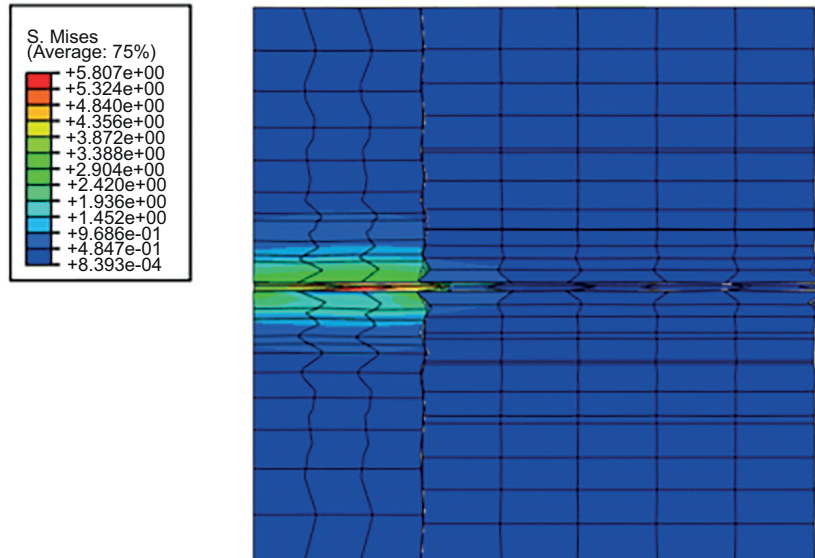


Fig. 23. The stress nephogram of the cementitious matrix.

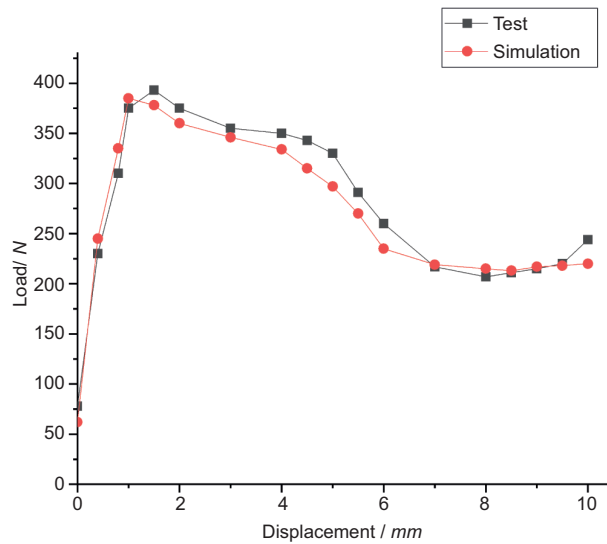


Fig. 24. The simulated load-displacement curve of the steel fiber drawing.

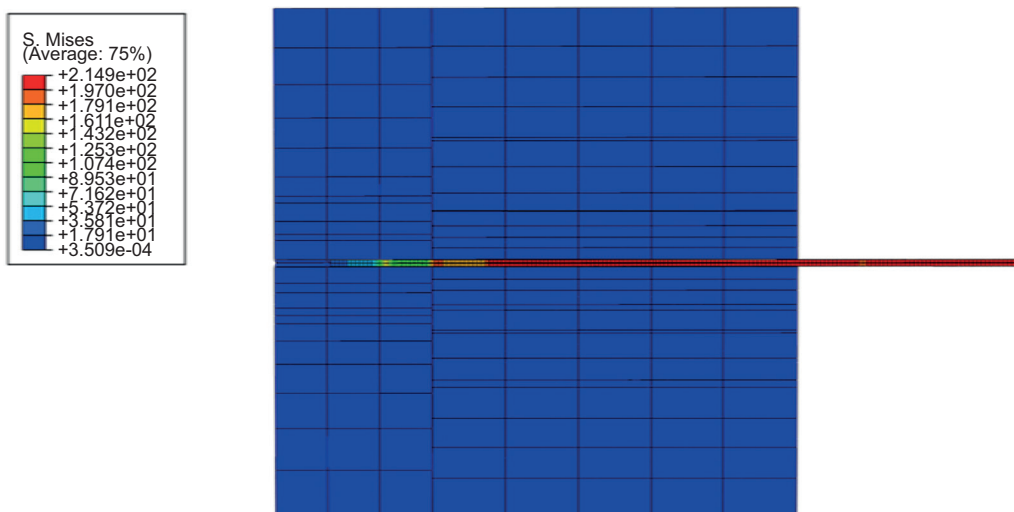


Fig. 25. The stress nephogram of the steel fiber drawing numerical simulation (20 mm).

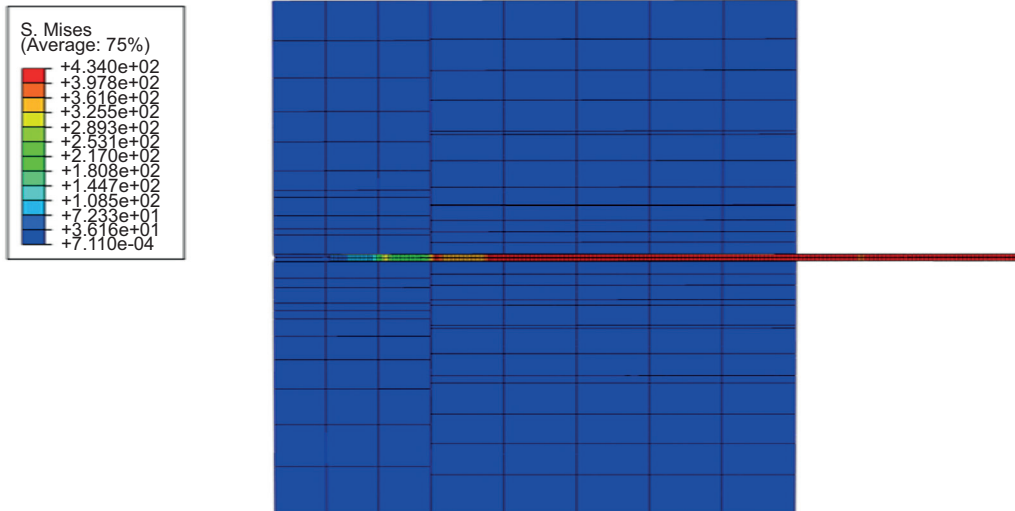


Fig. 26. The stress nephogram of the steel fiber drawing numerical simulation (40 mm).

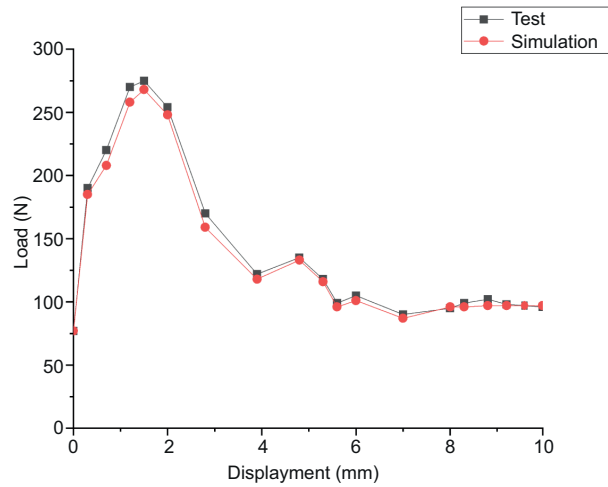


Fig. 27. The simulated load-displacement curve of the steel fiber drawing (20 mm).

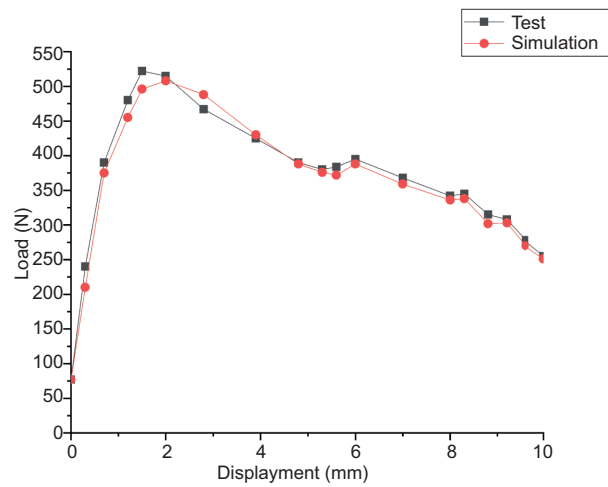


Fig. 28. The simulated load-displacement curve of the steel fiber drawing (40 mm).

from the matrix, it is found that the experimental test results are moderately different from those obtained by numerical simulation; however, the overall agreement is reasonable and acceptable. The overall deviation analyses are summarized as follows.

(1) The experimental data were inherently random to some extent. The fiber will not be preset during the drawing process and will bear the mechanical occlusal action of sand particles on the fiber during the drawing process.

(2) In the presented numerical model, the stress at the interface of the steel fiber increases gradually from the top to the bottom in the process of pull-out, and the pulling force is not uniformly sustained.

CONCLUSIONS

In this paper, the bond properties of industrial recycled steel fibers and the cementitious matrix are analyzed by experimental program and numerical simulation. Based on our investigation, the following conclusions are drawn:

- (1) The bond strength of the recycled steel fiber reinforced concrete cubes increases rapidly with the rise of the embedded depth of steel fiber and grows gently with the increase of inclined angle. The bonding strength of the special-shaped recycled steel fiber to the matrix is higher than that of straight round steel fiber, and the bonding strength of hook shaped recycled steel fiber in the special-shaped category is the highest. Among these factors, the specific shape of steel fiber has the paramount influence on the bonding strength and the ultimate tensile load, followed by the buried depth and embedment angle.
- (2) The phenomenon and mechanism of the interfacial pull-out failure are analyzed. Based on the analysis of the phenomena and the experimental curves, it is concluded that the pull-out process of the recycled steel fiber can be divided into three stages: (i) the full elastic restraint stage, (ii) the partial debonding stage, and (iii) the full debonding stage. When the steel fiber encounters the debonding failure, the damage of round straight recycling steel fiber is more serious than that of the special-shaped recycling steel fiber.
- (3) Based on the calculations of the change of bonding stress with slip in the anchorage zone, it is concluded that the distribution curve of the bonding stress of the recycled steel fiber along the anchorage length is similar to that of the

regular steel fiber, which is the same as the multi-peak curve, and the second peak is slightly lower than the first peak. The slippage of the round straight recycled steel fiber along the anchorage length occurs earlier than that of the special-shaped steel fiber. The high bond stress of the anisotropic steel fiber is longer than that of the round straight steel fiber, and the bond stress is fuller. The results reveal that the bonding stress of the recycled steel fiber increases curvilinearly with the rise of the anchorage depth in concrete. It is exhibited that the recycled steel fiber and the cementitious matrix can be reliably bonded together, the two phases are under common stresses, and the bonding performance between the two is good and satisfactory.

- (4) The numerical simulation and experiment show that the model has high prediction accuracy. The feasibility of replacing regular steel fiber in concrete with circulating steel fiber is further verified and the expected bonding effect between industrial regenerated steel fiber and cementitious matrix is achieved. The industrial recycled steel fibers are a class of “green” materials extracted from waste tires. The experimental program has opened a new technique for recycling waste tire wire line reuse, played a positive role in promoting the reuse of old tires, which will promote the process of solid waste recycling and laid a foundation for the subsequent study of other mechanical properties of recycled steel fibers.

OUTLOOK

In this paper, only pull-out tests were conducted to study the bonding performance of a single green fiber to concrete. The strength of the strengthening ability of the green steel fiber to the whole concrete specimen is not known, so further research is needed. In addition, the bead wire can be processed to make steel fiber mesh, and the mesh will be bonded to the bottom of the concrete slab or beam to study its strengthening reinforcement effect on the tensile zone of the slab or beam structure.

ACKNOWLEDGMENT

This work has been supported by the national key research and development plan project (No. 2017YFC0806100), the key research and

development project (No. 20200403161SF) of the science and Technology Department of Jilin Province.

DATA AVAILABILITY

All data generated or analyzed during this study are included in this published article.

CONFLICTS OF INTEREST

The authors declare that they have no conflicts of interest.

AUTHORS' CONTRIBUTIONS

Theoretical analysis: Yan LI, Wen-Yang DONG; Experimental analysis: Lan-qing SHI; Experimental setup: Xiao-peng WANG.

REFERENCES

- Aiello M.A., Leuzzi F., Centonze G. and Maffezzoli A. (2008). Use of steel fibres recovered from waste tyres as reinforcement in concrete: Pull-out behaviour, compressive and flexural strength. *Waste Management* 29 (6), 1960-1970. <https://doi.org/10.1016/j.wasman.2008.12.002>
- Aslani F. and Nejadi S. (2012). Bond characteristics of steel fiber and deformed reinforcing steel bar embedded in steel fiber reinforced self-compacting concrete (sfrsc). *Central European Journal of Engineering* 2 (3), 445-470. <https://doi.org/10.2478/s13531-012-0015-3>
- Chen G., Li Y. and Lin C.D. (2018). Experimental study on flexural performance of industrial recycled steel fiber reinforced concrete. *Proceedings of the 27th National Academic Conference on Structural Engineering (Volume II)*, 592-596.
- Deng F., Ding X. and Chi Y. (2018). The pull-out behavior of straight and hooked-end steel fiber from hybrid fiber reinforced cementitious composite: experimental study and analytical modelling. *Composite Structures* 206 (Dec.), 693-712. <https://doi.org/10.1016/j.compstruct.2018.08.066>
- Garcia-Taengua E., Martí-Vargas J.R. and Serna P. (2016). Bond of reinforcing bars to steel fiber reinforced concrete. *Construction and Building Materials* 105 (Feb.15), 275-284. <https://doi.org/10.1016/j.conbuildmat.2015.12.044>
- Hamoush S., Abu-Lebdeh T., Cummins T. and Zorning B. (2010). Pullout characterizations of various steel fibers embedded in very high strength concrete. *American Journal of Engineering and Applied Sciences* 3(2), 418. <https://doi.org/10.3844/ajeassp.2010.418.426>
- Hou L., Ye Z., Zhou B., Shen C. and Chen D. (2019). Bond behavior of reinforcement embedded in steel fiber reinforced concrete under chloride attack. *Structural Concrete* 20 (6), 2242-2255 <https://doi.org/10.1002/suco.201800246>
- Hong X.J. and Zhang Y. (2000). Fitting method of bond stress in bond slip test. *Structural Engineer* 15 (3). <https://doi.org/10.3969/j.issn.1005-0159.2000.03.011>
- Jiang Q.R., Li Y. and Fang Q. (2018). Experimental study on shear and splitting tensile properties of industrial recycled steel fiber reinforced concrete. *Proceedings of the 27th National Academic Conference on Structural Engineering (Volume II)*, 581-586.
- Krenchel H. and Shah S.P. (1985). Fracture analysis of the pullout test. *Materials and Structures* 18 (6), 439-446. <https://doi.org/10.1007/BF02498746>
- Khaloo A.R. and Kim N. (1996). Mechanical properties of normal to high-strength steel fiber-reinforced concrete. *Cement Concrete and Aggregates* 18 (2). <https://doi.org/10.1520/CCA10156J>
- Katz A. and Li V.C. (1995). Inclination angle effect of carbon fibers in cementitious composites. *Journal of Engineering Mechanics* 121 (12), 1340-1349. [https://doi.org/10.1061/\(ASCE\)0733-9399\(1995\)121:12\(1340\)](https://doi.org/10.1061/(ASCE)0733-9399(1995)121:12(1340))
- Lee Y., Kang S.T. and Kim J.K. (2010). Pullout behavior of inclined steel fiber in an ultra-high strength cementitious matrix. *Construction and Building Materials* 24 (10), 2030-2041. <https://doi.org/10.1016/j.conbuildmat.2010.03.009>
- Li C.Y. and Mobasher B. (2015). Finite element simulations of fiber pullout toughening in fiber reinforced cement based composites. *Advanced Cement Based Materials* 7(3-4). [https://doi.org/10.1016/S1065-7355\(97\)00087-4](https://doi.org/10.1016/S1065-7355(97)00087-4)
- Li Y., Zhang Y.M. and Wang T.H. (2018). Experimental study on modulus of elasticity and splitting tensile strength of concrete after high temperature (fire) with different cooling modes. *Proceedings of the 27th National Academic Conference on Structural Engineering Structural Engineering Professional Committee of Chinese Mechanics Society Xi'an, China October 13th*, 331-335 (Volume I), 331-335.
- Mo K.H., Goh S.H., Alengaram U.J., Visintin P. and Jumaat M.Z. (2017). Mechanical, toughness, bond and durability-related properties of lightweight concrete reinforced with steel fibres. *Materials and Structures* 50, 46. <https://doi.org/10.1617/s11527-016-0934-1>

- Song P.S., Hwang S. (2004). Mechanical properties of high-strength steel fiber-reinforced concrete. *Construction and Building Materials* 18 (9), 669-673. <https://doi.org/10.1016/j.conbuildmat.2004.04.027>
- Thomas J. and Ramaswamy A. (2007). Mechanical properties of steel fiber-reinforced concrete. *Journal of Materials in Civil Engineering* 19 (5), 385-392. [https://doi.org/10.1061/\(ASCE\)0899-1561\(2007\)19:5\(385\)](https://doi.org/10.1061/(ASCE)0899-1561(2007)19:5(385))
- Xu B.W., Ju J.W. and Shi H.S. (2011). Progressive micro-mechanical modeling for pullout energy of hooked-end steel fiber in cement-based composite. *International Journal of Damage Mechanics* 20 (6), 922-938. <https://doi.org/10.1177/1056789510385260>
- Xu B.W., Ju J.W. and Shi H.S. (2012). Micromechanical modeling of fracture energy for hooked-end steel fiber reinforced cementitious composites. *International Journal of Damage Mechanics* 21(3), 415-439. <https://doi.org/10.1177/1056789510397072>
- Yue L.I., Xinglei W. and Qingjun D. (2017). Study on properties of steel fiber reinforced concrete. *Concrete* 20 (6), 922-938. <https://doi.org/10.1177/1056789510385260>
- Zhou M.K., Lu Z.A., Wan H.Q. and Li L.J. (2000). The flexural strength and reinforcing mechanism of the top-and-bottom-layered steel fiber concrete. *Journal of Wuhan University of Technology-Materials Science* 15 (2), 21-27,34.
- Zhang G.Q., Suwatnodom, P. and Ju, J.W. (2013). Micro-mechanics of crack bridging stress-displacement and fracture energy in steel hooked-end fiber reinforced cementitious composites. *International Journal of Damage Mechanics* 22 (6), 829-859. <https://doi.org/10.1177/1056789512468356>
- Zile E. and Zile O. (2013). Effect of the fiber geometry on the pullout response of mechanically deformed steel fibers. *Cement and Concrete Research* 44, 18-24. <https://doi.org/10.1016/j.cemconres.2012.10.014>
- Zhang Y., Ju J.W., Zhu H.H., Chen Q., Guo Q.H. and Yan Z.G. (2019). A novel damage model based on micromechanics for hybrid fiber reinforced cementitious composites under uniaxial compression. *International Journal of Damage Mechanics* 28(7), 1095-1132. <https://doi.org/10.1177/1056789518813270>
- Zhang Y., Ju J.W., Zhu H.H. and Yan Z.G. (2020). A novel multi-scale model for predicting the thermal damage of hybrid fiber reinforced concrete. *International Journal of Damage Mechanics* 29(1), 19-44. <https://doi.org/10.1177/1056789519831554>